Supplemental materials for

Structure of a dominant-negative helix-loop-helix transcriptional regulator suggests mechanisms of autoinhibition

Ryohei Ishii, Kazunobu Isogaya, Azusa Seto, Daizo Koinuma, Fumio Arisaka, Yuji Watanabe, So-ichi Yaguchi, Hiroaki Ikushima, Naoshi Dohmae, Kohei Miyazono, Keiji Miyazawa, Ryuichiro Ishitani and Osamu Nureki

Supplementary Discussion

Structural reorganization of the N and C bundles upon dissociation from the HLH region

To further analyze the dynamic equilibrium between the V-shaped and relaxed forms, we performed molecular dynamics (MD) simulations of HHM starting from the present crystal structure, with and without the HLH region.

In the 100-ns trajectory of full-length HHM, a small hinge-bending motion between the C and N bundles was observed, but the V-shaped conformation was stable, maintaining the interaction between Asp275 and Thr113, and no large structural reorganization was observed (run F; Supplementary Figure S7A). In contrast, in the simulations without the HLH region, the arrangement of the N and C bundles drastically changed after tens of nanoseconds (Supplementary Figure S7A and B). We performed three independent simulations without the HLH region, and all of them consistently

showed a similar tendency toward the drastic change in the N and C bundle arrangement, with the disruption of the interactions between Asp275, Ile112 and Thr113. In run B, the arrangement of the N and C bundles slightly changed, and resulted in the V-shaped four-helix bundles similar to the initial structure (Supplementary Figure S7C). In contrast, in the other two simulations (runs A and C), the hydrophobic residues that were originally involved in the interaction with the HLH region formed new interactions between the N and C bundles, potentially creating a reorganized eight-helix bundle (Supplementary Figure S7C). These results from the simulation are apparently contradictory to the results from the pull-down assay (Figure 5B), which showed the dissociation of the N and C bundles in this dynamic equilibrium (Figure 4B). However, it is possible that the formation of the transient eight-helix bundle, as observed in the simulation, occurs as an early event in the slow structural conversion to the relaxed form, since the MD simulation can prove events that occur in a sub-microsecond order timescale.

Supplementary Methods

Molecular dynamics simulation

The initial structure for the simulation of the full-length HHM (run F) was built from the crystal structure of HHM. The short disordered loops, L1 (41–44) and L9 (329–333), were modeled by the program MODELLER (Sanchez & Sali, 1997). The long loops L4 and L6, which are completely disordered in the crystal structure, were not included in the simulation system. The protonation states of the Asp, Glu, and His residues were determined using the program PDB2PQR (Dolinsky et al, 2007). All water molecules observed in the crystal structure were kept. Hydrogen atoms were added by using the psfgen plugin of VMD (Humphrey et al, 1996). The system was then solvated to form a 96×96×96 Å simulation box with 28,146 TIP3P water molecules, by using the solvate plugin of VMD. The resulting solvated system was neutralized by randomly adding 47 Na^+ and 33 Cl^- ions in the bulk water. MD simulations were performed using the NAMD 2.7 package (Phillips et al, 2005) on the RIKEN Integrated Cluster of Clusters (RICC), RIKEN (Wako, Japan). The CHARMM27 set of force field parameters (MacKerell et al, 1998) with ϕ, ψ cross term map (CMAP) correction (Mackerell et al, 2004) and the TIP3P model (Jorgensen et al, 1983) were used for protein and water molecules, respectively. Bond lengths between hydrogens and heavy atoms were restrained by the RATTLE method (Andersen, 1983), allowing an integration step of 2 fs. The target pressure and temperature were set to 1.0 atm and 300 K, respectively. Constant pressure was maintained by using the Langevin piston Nose-Hoover method (Feller et al, 1995; Martyna et al, 1994). A Langevin damping coefficient, γ, of 5.0 ps^{-1} was used for temperature control. Periodic boundary

conditions were implemented in all systems. The particle mesh Ewald (PME) method (Darden et al, 1993) was employed to calculate electrostatic forces without truncation. The initial structures were subjected to energy minimization to remove unfavorable contacts. The systems were then relaxed by 10-ns MD simulations with positional constraints of 10.0 kcal mol^{-1} $Å^{-2}$ on the protein main-chain heavy atoms, which were gradually removed with a subsequent 1-ns simulation. Finally, we performed a 100-ns simulation with no restraints.

The initial structure of the simulation of HHM without the HLH region was built as described above, after removing the HLH region (151–200) from the crystal structure. We conducted three simulation runs (A, B, and C) without the HLH region, as follows. In run A, we utilized a different simulation box, 64×128×128 Å, including 34,086 water molecules, 52 Na^+ ions, and 43 Cl^- ions. In runs B and C, we utilized the same simulation box as in run F, including 28,410 water molecules, 44 Na^+ ions, and 35 Cl^- ions. The simulation systems were subjected to energy minimization, and were then relaxed by 9-ns (run C) and 10-ns (runs A and B) simulations with positional constraints of 10.0 kcal mol^{-1} $Å^{-2}$ on the protein main-chain heavy atoms, which were gradually removed with subsequent 1-ns simulations. Finally, we performed 100-ns simulations with no restraints.

Supplementary Figure Legends

Sup. Fig. S1. Mutated Cys residues for crystal quality improvement.

(A) Overall and (B) close-up views of the mutated Cys198 and Cys300 residues of HHM.

Sup. Fig. S2. Putative LZ motif involved in the C-bundle formation.

Sup. Fig. S3. $2F_o-F_c$ electron density map between the N terminus of α6 and the N and C bundles at the edge of the V-shape

Sup. Fig. S4. Molecular surface of HHM.

(A) The surface electrostatic potential of HHM. The positively charged regions are colored blue and the negatively charged regions are colored red, with the intensity of the color proportional to the local potential (range –10 kT/e to +10 kT/e). (B) The hydrophobic residues exposed on the surface of HHM. The hydrophobic residues (i.e. Ile, Val, Leu, Met, Phe, Trp) are colored gray and the other residues are colored cyan.

Sup. Fig. S5. Analytical ultracentrifugation of HHM.

The raw absorbance distributions and the best-fit model calculated by the SEDFIT program (top). Residuals of the fit (middle), sedimentation coefficients, c(s), and distributions (bottom) of wild type HHM (A), N169E mutant HHM (B), and P166Y mutant HHM (C).

Sup. Fig. S6. HHM and the HHM mutants failed to interact with MyoD.

COS7 cells were transfected with the indicated plasmids (FLAG-tagged HHM or HHM mutants and 6myc-tagged MyoD or Olig1). HHM and its mutants were immunoprecipitated (IP), and the co-precipitated proteins were visualized by immunoblotting (top panel). Input of MyoD or Olig1 (second panel), HHM and its mutants (third panel), are also shown. HHM and the four HHM mutants failed to interact with MyoD. Olig1 was used as a positive control.

Sup. Fig. S7. Molecular dynamics simulations of HHM with and without the HLH region.

(A) Plots of the RMSD values from the crystal structure against time, during the simulations (runs F, A, B, and C). The RMSD values were calculated for the Cα atoms of the helices in the N and C bundles (i.e. helices α1–4, and α7–8). (B) Helix-bundle rotation as a function of time during the simulations (runs F, A, B, and C). The helix-bundle rotation angle was calculated by fitting the N bundle and then measuring the rotation angle of the C bundle with respect to the crystal structure. (C) Final snapshot structures from the simulation runs A, B, and C (purple, pink, and khaki, respectively). The protein main chains are fitted on the N bundle in the crystal structure, and are shown by tube models. For comparison, the present crystal structure is shown in cyan. The structures are viewed from two perpendicular directions.

References

Andersen HC (1983) Rattle - A Velocity Version Of The Shake Algorithm For Molecular-Dynamics Calculations. *J Comput Phys* **52**(1)**:** 24-34

Darden T, York D, Pedersen L (1993) Particle Mesh Ewald - An N.Log(N) Method For Ewald Sums In Large Systems. *J Chem Phys* **98**(12)**:** 10089-10092

Dolinsky TJ, Czodrowski P, Li H, Nielsen JE, Jensen JH, Klebe G, Baker NA (2007) PDB2PQR: expanding and upgrading automated preparation of biomolecular structures for molecular simulations. *Nucleic Acids Res* **35:** W522-W525

Feller SE, Zhang YH, Pastor RW, Brooks BR (1995) Constant-Pressure Molecular-Dynamics Simulation - The Langevin Piston Method. *J Chem Phys* **103**(11)**:** 4613-4621

Humphrey W, Dalke A, Schulten K (1996) VMD: Visual molecular dynamics. *J Mol Graph* **14**(1)**:** 33-38

Jorgensen WL, Chandrasekhar J, Madura JD, Impey RW, Klein ML (1983) Comparison Of Simple Potential Functions For Simulating Liquid Water. *J Chem Phys* **79**(2)**:** 926-935

MacKerell AD, Bashford D, Bellott M, Dunbrack RL, Evanseck JD, Field MJ, Fischer S, Gao J, Guo H, Ha S, Joseph-McCarthy D, Kuchnir L, Kuczera K, Lau FTK, Mattos C, Michnick S, Ngo T, Nguyen DT, Prodhom B, Reiher WE, Roux B, Schlenkrich M, Smith JC, Stote R, Straub J, Watanabe M, Wiorkiewicz-Kuczera J, Yin D, Karplus M (1998) All-atom empirical potential for molecular modeling and dynamics studies of proteins. *J Phys Chem B* **102**(18)**:** 3586-3616

Mackerell AD, Feig M, Brooks CL (2004) Extending the treatment of backbone

energetics in protein force fields: Limitations of gas-phase quantum mechanics in reproducing protein conformational distributions in molecular dynamics simulations. *J Comput Chem* **25**(11)**:** 1400-1415

Martyna GJ, Tobias DJ, Klein ML (1994) Constant-Pressure Molecular-Dynamics Algorithms. *J Chem Phys* **101**(5)**:** 4177-4189

Phillips JC, Braun R, Wang W, Gumbart J, Tajkhorshid E, Villa E, Chipot C, Skeel RD, Kale L, Schulten K (2005) Scalable molecular dynamics with NAMD. *J Comput Chem* **26**(16)**:** 1781-1802

Sanchez R, Sali A (1997) Evaluation of comparative protein structure modeling by MODELLER-3. *Proteins***:** 50-58

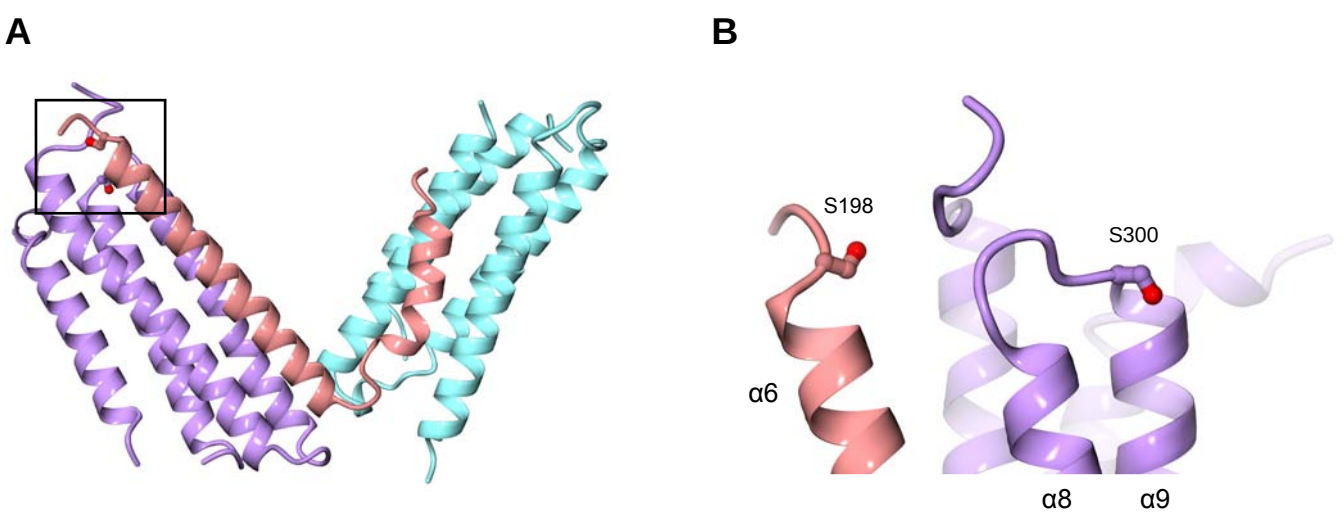

Sup. Fig. S1

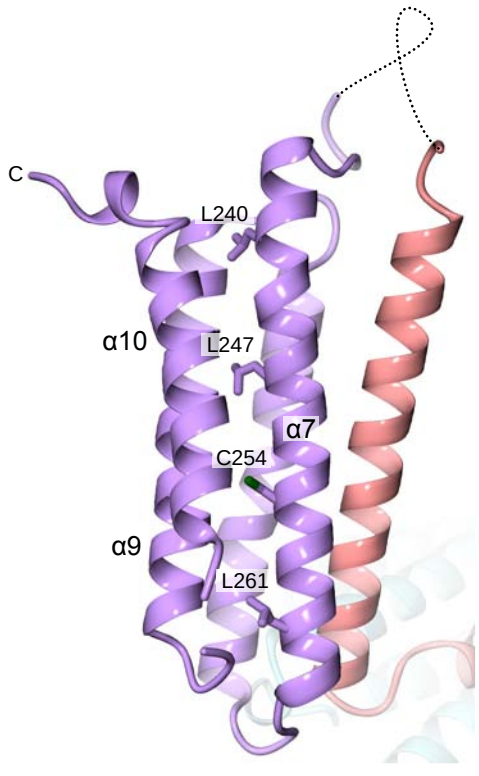

C bundle

Sup. Fig. S2

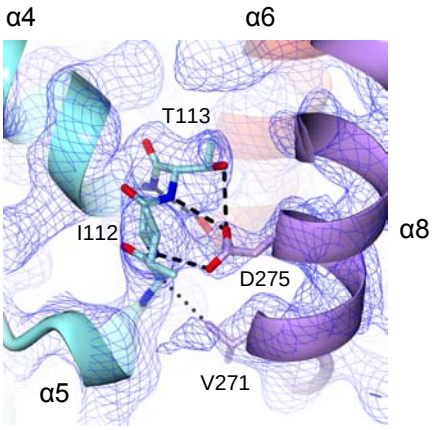

Sup. Fig. S3

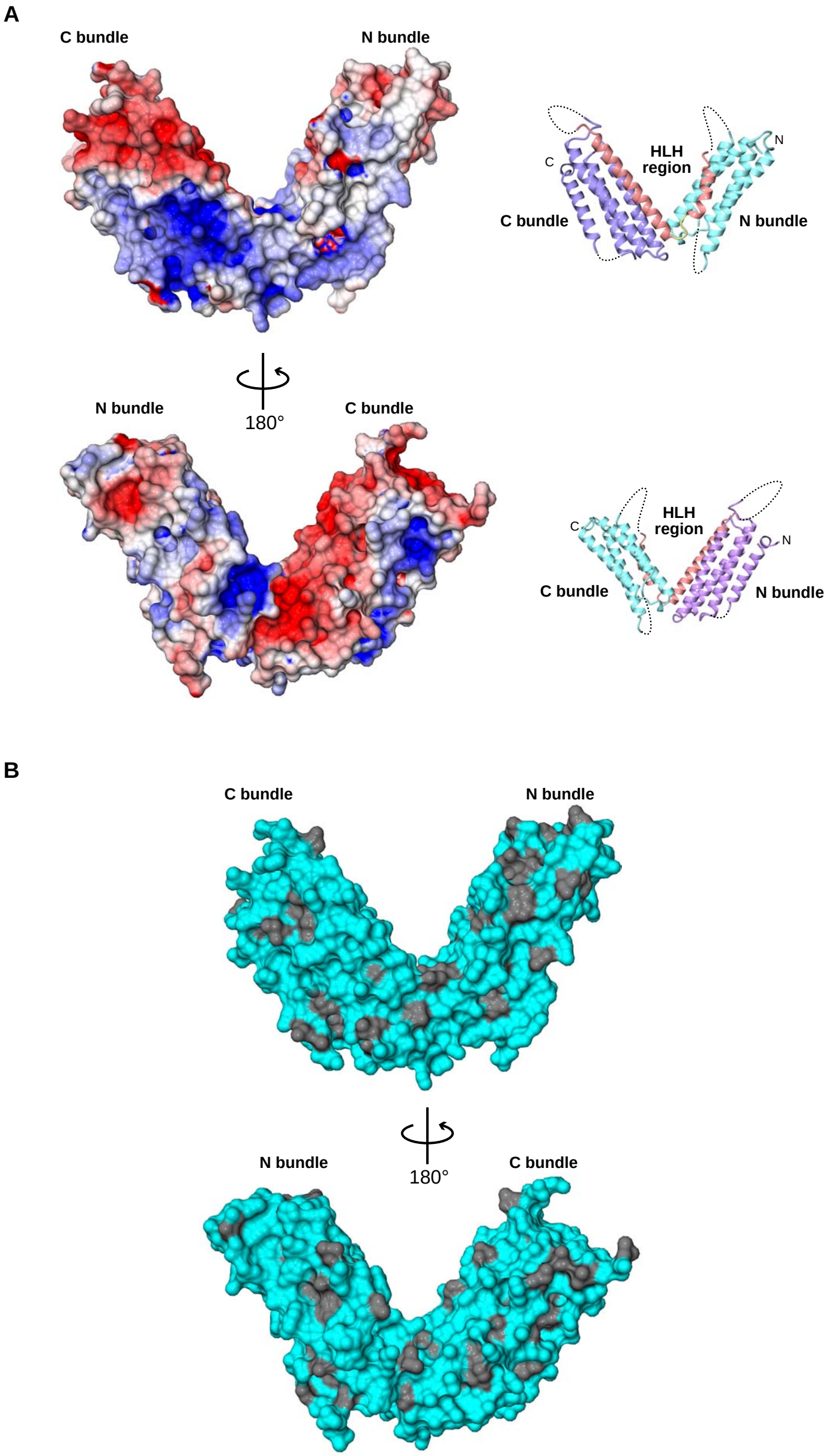
A
C bundle
N bundle
C
HLH
region
N
C bundle
N bundle
N bundle
C bundle
180°
C
HLH
region
N
C bundle
N bundle
B
C bundle
N bundle
N bundle
C bundle
180°

Sup. Fig. S4

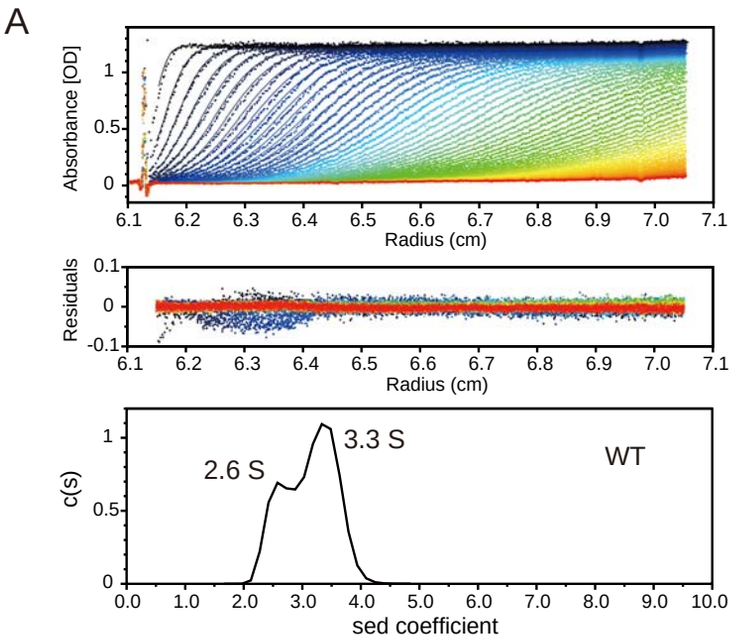
A
Absorbance [OD]
Radius (cm)
Residuals
Radius (cm)
c(s)
2.6 S
3.3 S
WT
sed coefficient

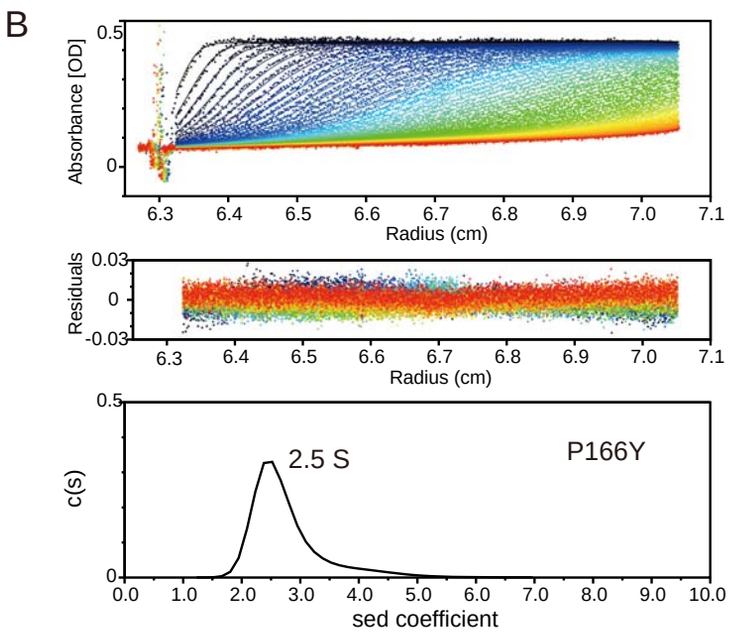
B
Absorbance [OD]
Radius (cm)
Residuals
Radius (cm)
c(s)
2.5 S
P166Y
sed coefficient

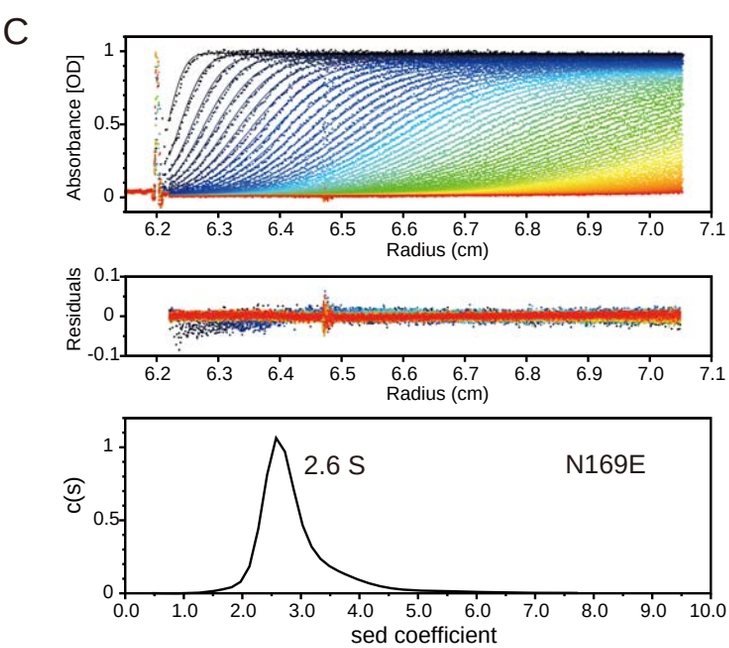
C
Absorbance [OD]
Radius (cm)
Residuals
Radius (cm)
c(s)
2.6 S
N169E
sed coefficient

Sup. Fig. S5

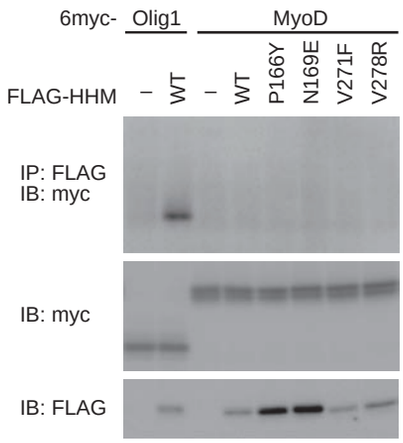
6myc-
Olig1
MyoD
FLAG-HHM
–
WT
–
WT
P166Y
N169E
V271F
V278R
IP: FLAG
IB: myc
IB: myc
IB: FLAG

Sup. Fig. S6

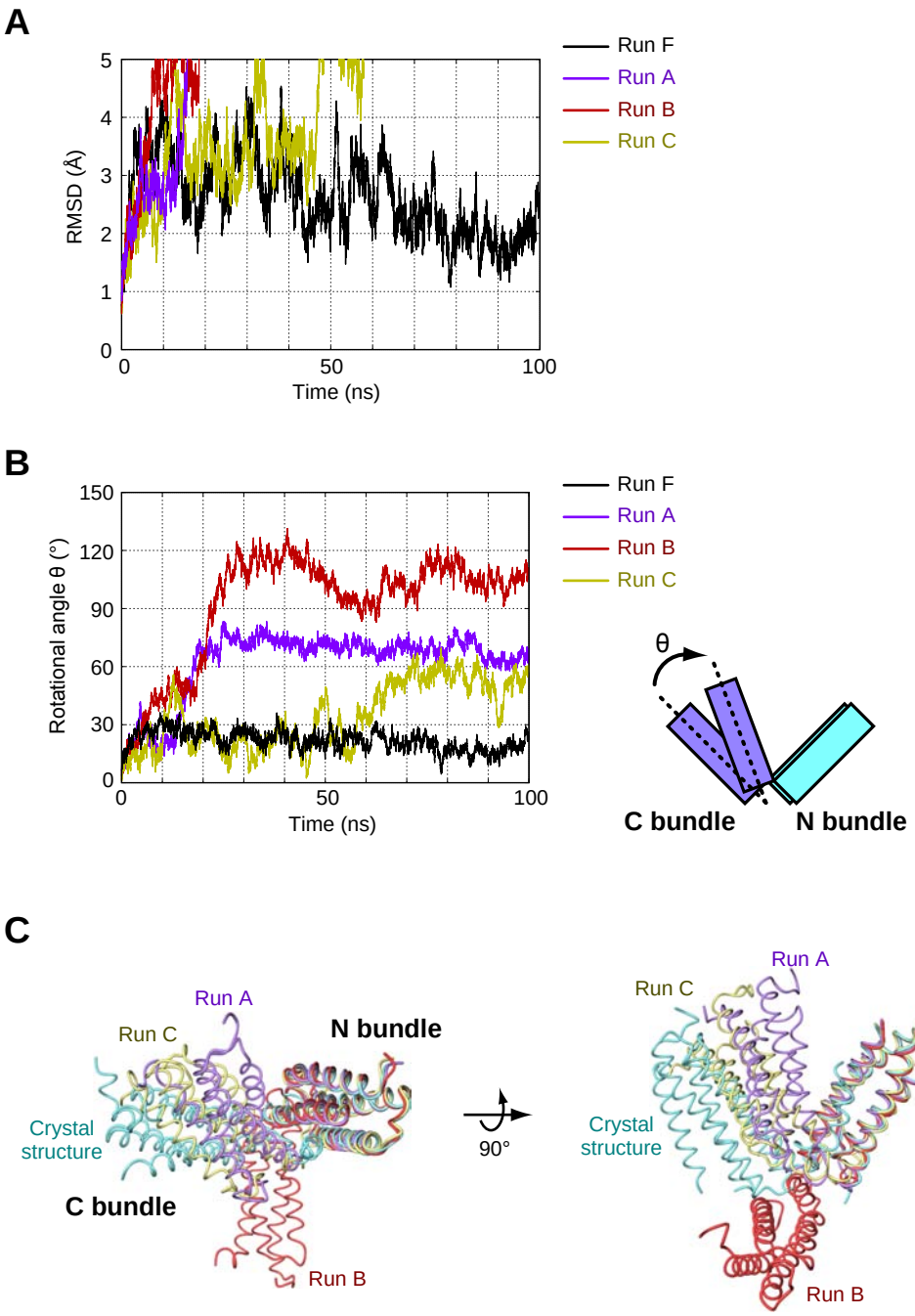
A
RMSD (Å)
Time (ns)
Run F
Run A
Run B
Run C
B
Rotational angle θ (°)
Time (ns)
Run F
Run A
Run B
Run C
θ
C bundle
N bundle
C
Run A
Run C
N bundle
Crystal structure
C bundle
Run B
90°
Run A
Run C
Crystal structure
Run B

Sup. Fig. S7